Scientific Reports

https://doi.org/10.1038/s41598-026-41288-7

Article in Press

The 129S1/SvlmJ mouse strain recapitulates severe hypertensive target organ damage under moderate angiotensin II–induced hypertension

Received: 14 October 2025

Accepted: 19 February 2026

Published online: 05 March 2026

Cite this article as: Orieux A., Boulestreau R., Bats M. *et al.* The 129S1/SvlmJ mouse strain recapitulates severe hypertensive target organ damage under moderate angiotensin II–induced hypertension. *Sci Rep* (2026). https://doi.org/10.1038/s41598-026-41288-7

Arthur Orieux, Romain Boulestreau, Marie-Lise Bats, Maxime Michot, Alexandre Boyer, Virginie Dinet, Juliette Vaurs, Pascale Dufourcq, Claire Peghaire, Cécile Duplaa, Thierry Couffinhal & Sébastien Rubin

The 129S1/SvlmJ mouse strain recapitulates severe hypertensive target organ damage under moderate angiotensin II–induced hypertension

Arthur ORIEUX[1, 2] (MD), Romain BOULESTREAU[1,3] (MD), Marie-Lise BATS[1,4] (PharmD, PhD), Maxime MICHOT[1] (MD), Alexandre BOYER (MD, PhD)[2], Virginie DINET[1] (PhD), Juliette VAURS[1] (MS), Pascale DUFOURCQ[1], Claire PEGHAIRE[1] (PharmD, PhD), Cécile DUPLAA[1] (PhD), Thierry COUFFINHAL[1,3] (MD, PhD), Sébastien RUBIN*[1,5] (MD, PhD)

[1] Univ. Bordeaux, INSERM, BMC, U1034, F-33600 Pessac, France

[2] Service de Médecine Intensive Réanimation, CHU de Bordeaux, Bordeaux, France

[3] Service des Maladies Coronaires et Vasculaires, CHU de Bordeaux, 1, Avenue de Magellan, Hôpital Haut Lévêque, Pessac F-33604, France.

[4] Service de Biochimie, CHU de Bordeaux, Bordeaux, France

[5] Service de Néphrologie, Transplantation, Dialyse et Aphérèses, CHU de Bordeaux, Bordeaux, France

Corresponding author: Pr. Sébastien RUBIN, sebastien.rubin@chu-bordeaux.fr

SHORT TITLE : 129S1 Mouse: Genetic Susceptibility to Hypertension

WORDS COUNT : 6029

Abstract

Aim

Hypertension remains the leading cause of cerebral, cardiac, renal, and retinal vascular damage. However, genetic determinants underlying organ-specific vulnerability are poorly understood, and commonly used mouse models, notably C57BL/6J, often fail to recapitulate severe hypertensive complications seen in humans. This study compares the widely used C57BL/6J mouse strain with the genetically distinct 129S1/SvlmJ strain under hypertensive stress, aiming to identify a model that better reproduces hypertensive target organ damage.

Methods and Results

Moderate hypertension was induced in 129S1/SvlmJ and C57BL/6J mice using chronic infusion of angiotensin II (600 ng/kg/min). Despite comparable blood pressure elevations, only 129S1/SvlmJ mice developed severe organ damage, including cognitive impairment, pronounced blood-brain barrier disruption, retinal vasculopathy, cardiac hypertrophy, and podocyte lesions with albuminuria. In contrast, C57BL/6J mice exhibited markedly less organ injury under the experimental conditions tested. Transcriptomic analysis of cerebral microvessels identified distinct inflammatory and immune-related signatures between strains, paralleling their vascular phenotypes. These immune profiles appear as hallmarks of strain-specific susceptibility rather than as direct protective or deleterious mechanisms.

Conclusion

This study demonstrates that genetic background critically shapes hypertensive complications, identifying the 129S1/SvlmJ strain as a relevant and translational model of hypertensive target organ damage. Beyond reproducing key features of severe hypertension, this model provides a framework to investigate the pathways linking genetic susceptibility, vascular injury, and end-organ damage.

I. Introduction

Hypertension affects over 1.5 billion individuals globally and remains the leading modifiable risk factor for cardiovascular and renal diseases[1]. It is also the leading chronic risk factor for years of life lost, accounting for roughly 200 million years lost per year[2,3]. This leads to severe complications such as cerebral small vessel disease (cSVD), cognitive impairment, chronic kidney disease (CKD), and progressive renal failure. Indeed, even with optimal blood pressure control, many patients continue to develop severe complications, while others remain largely unaffected, suggesting important mechanisms independent of the mechanical effects of hypertension. The precise factors determining organ-specific susceptibility and resilience to hypertensive damage, particularly in the brain and kidneys, are poorly understood. Understanding these determinants requires experimental models that faithfully reproduce organ-specific hypertensive complications[4].

In the pursuit of identifying the mechanistic determinants of organ-specific vulnerability, Genome-wide association studies (GWAS) in humans have identified genetic polymorphisms associated with hypertension and its complications[5]. Yet, translating these findings into mechanistic insights has been challenging. GWAS provide limited causal understanding, and clinical studies often cannot manipulate specific pathways experimentally[6]. Consequently, preclinical models are essential for exploring the biological processes underlying hypertensive complications. While mouse models remain invaluable tools in hypertension research, existing models often fail to replicate the complexity of human hypertension and its diverse organ-specific damage[7]. Furthermore, the influence of genetic background on the severity and pattern of hypertensive target organ injury remains insufficiently captured by current mouse models.

To address this gap, robust and physiologically relevant mouse models are needed to investigate hypertensive complications. We examined how genetic background affects hypertensive complications

using a model of moderate hypertension induced by angiotensin II (AngII). By comparing two genetically distinct mouse strains—129S1/SvlmJ (129/Sv) and C57BL/6J—we observed striking differences in the severity and patterns of organ-specific damage. Notably, 129/Sv mice exhibited extensive damage to the brain, kidneys, retina, and heart, reflecting severe hypertensive complications in humans. In contrast, C57BL/6J mice appeared to be protected from such damage. Our findings suggest that the C57BL/6J strain, despite its widespread use, may be suboptimal for modeling hypertensive target organ damage, whereas the 129S1/SvlmJ strain more faithfully reproduces severe complications. Transcriptomic analyses revealed distinct inflammatory signatures associated with strain-specific patterns of injury, underscoring the potential of this comparative approach to dissect genetic and molecular determinants of hypertensive complications.

II. Methods

Animals

129S1/SvlmJ (129/Sv) mice were obtained from *Charles River Laboratories*, strain code 287, while C57BL/6J mice were sourced from *The Jackson Laboratory,* strain code 000664. The mice are maintained on a standard laboratory diet (SAFE A04, Safe Laboratory, France) and are housed in a specific pathogen-free environment.

Unless otherwise specified, all experiments were performed in male mice. A separate female cohort was used exclusively for confirmatory assessment of selected phenotypes (cardiac hypertrophy, albuminuria, and BBB permeability).

The animals were housed in a conventional facility on a 12-hour (light/dark) cycle, with water and food provided ad libitum. At the end of the experiment, mice were euthanized by intraperitoneal injection of ketamine (150 mg/kg) and xylazine (10 mg/kg). Depending on the planned analyses, animals subsequently underwent either cervical dislocation or transcardiac perfusion with phosphate-buffered saline to clear the vasculature.

This study was conducted in accordance with the local Animal Care and Use Committee at Bordeaux University (Committee CEEA50, approval number : 20210609181238 36) and the regulations in effect within the European Community for experimental animal use (L358-86/609/EEC). General surgical procedures were performed on mice (ages 3–12 months, weights 25–35 g) following the ARRIVE guidelines (https://www.nc3rs.org.uk/arrive-guidelines).

AngII-induced hypertension

Moderate hypertension was induced in three-month-old male mice by subcutaneous infusion of angiotensin II (AngII, Sigma-Aldrich, USA; A9525-50MG) using osmotic pumps (ALZET 1004, Alzet, USA). The pumps were preloaded to deliver AngII at a rate of 600 ng/kg/min for 28 days (D28). Control mice (SHAM) received an equivalent saline infusion (0.9%). The day of pump implantation was designated as day 0 (D0). Mice were

anesthetized with 1.5% isoflurane in oxygen during pump implantation, and perioperative analgesia was provided through subcutaneous buprenorphine (0.05 mg/kg) (Ceva Santé Animale, Libourne, France). The pumps were implanted subcutaneously in the dorsal region to minimize handling stress. Mice were monitored postoperatively for recovery and weight stability. AngII/saline infusion procedures were identical in the female confirmatory cohort.

Blood pressure measurement

A catheter (PA-C10, AD Instrument, New Zealand) is inserted into the carotid artery, and the transmitter was placed subcutaneously. After five days, mice were placed onto RPC-1 Single Receiver (AD Instrument, New Zealand). Data were acquired every week over one hour during the day using LabChart software (v7, AD Instruments, New Zealand) to calculate mean systolic blood pressure (sBP).

Blood pressure was assessed using invasive radiotelemetry, with a catheter (PA-C10, AD Instrument, New Zealand) inserted into the carotid artery of freely moving mice to provide continuous, stress-free hemodynamic monitoring.

To ensure maximal reproducibility and facilitate accurate longitudinal tracking across large experimental cohorts, mean systolic blood pressure (sBP) was systematically calculated from standardized 1-hour recordings. These recordings were performed in a dedicated, standardized area during the light phase (between 10:00 AM and 11:00 AM), specifically targeting the peak of the 12-hour physiological inactivity and resting period in mice. This methodological choice was strictly validated by preliminary continuous 12-hour inactivity cycle telemetry recordings, which demonstrated that the systolic blood pressure values captured during this morning resting window were highly consistent with the average values measured over the entire circadian cycle, thereby ensuring that our 1-hour snapshot provides a reliable and representative estimate of the total hemodynamic load throughout the study.

Brain damage assessment

- **Behavioral test**

The Morris Water Maze (MWM) test was conducted from day 21 to 28 after hypertension onset, as previously described[8], to assess spatial learning and memory. Before testing, visual acuity was confirmed using the visual cliff test. Briefly, mice underwent four acquisition trials daily over four consecutive days, learning to locate a submerged platform. Latency to reach the platform was recorded, with shorter latencies indicating better performance. Three days later, memory retention was evaluated by a 90-second Probe Test without the platform, measuring mean proximity to the original platform location. All behavioral data were collected and analyzed using EthovisionXT v16 software (Noldus Information Technology, Wageningen, Netherlands)[8,9].

- **Cerebral blood flow**

Laser-Doppler imaging (MOORLDI2-IR™, Moor Instruments, UK) was used to measure cerebral blood flow (CBF) at baseline and after 28 days of infusion. Mice were anesthetized during measurements, and body temperature was maintained on a heating platform.

- **Blood-brain barrier permeability assessment *in vivo***

As previously described[10], mice were anesthetized, and 75 µl of TMR dextran 3 kDa lysine-fixable tracer (Texas Red™, 3000 MW, Lysine Fixable, ThermoFisher Scientific, Cat# D3328, MA, USA) was injected intravenously (retro-orbital). Twenty minutes later, a 300 µL blood sample was collected via cardiac puncture and centrifuged at 10,000 x g for 10 minutes at 4 °C to prepare the serum. The mice were euthanized immediately after collecting the blood sample. One hemibrain, devoid of olfactory lobes and cerebellum, was collected, and its weight was recorded before being snap-frozen in liquid nitrogen. Tissues were homogenized in cold 1X phosphate-buffered saline (PBS) using a Tissue Lyser (Qiagen, Germany) and centrifuged at 15,000 g for 20 minutes at 4 °C. The supernatant was then collected. Fluorescence measurement (RFUs) of 50

µL of diluted serum and brain supernatant was performed using a Spark® Multimode Microplate Reader (Tecan). We calculated a permeability index (PI) expressed in mL/g (tissue RFUs/g tissue weight) / (serum RFUs/mL serum) for each animal. The PI of each animal in the groups was divided by the mean PI of the SHAM group, setting the SHAM group mean to 1 while maintaining the inter-animal variation within the control group. This transformation yields values for the AngII group relative to the SHAM group, which is set to 1 for each strain.

- **Comprehensive three-dimensional analysis of brain (CUBIC)**

Mice were transcardially perfused with a wash solution (0.9% NaCl + heparin 20 U/mL) and then fixed using 4% PFA. Post-perfusion, the brains were harvested, and 400 µm-thick coronal sections of the parietal area were prepared using a vibratome.

The brain slices were subjected to tissue clearing and immunolabeling using the CUBIC method[11]. Briefly, the sections were incubated in progressive CUBIC-1 reagent concentration for 36 hours at 37°C to facilitate tissue clearing. After clearing, the slices were incubated with the primary antibody for 48 hours at 4°C with gentle shaking at 37°C. Then, brain slices were incubated with primary antibodies: GFAP (1:400, ThermoFisher Scientific, 130300, MA, USA), PODOCALYXIN (1:400, R&D Systems, AF1556, Minneapolis, MN, USA), IBA1 (1:400, Fujifilm Wako, 019-19741, Osaka, Japan), CD206 (1:400, R&D Systems, AF2535, Minneapolis, MN, USA). The slices were washed and incubated with the conjugated secondary antibodies (Alexa Fluor, ThermoFisher Scientific, MA, USA) under the same conditions for 48 hours. Finally, the slices underwent a second clearing step using progressive CUBIC-2 reagent concentration for 36 hours at room temperature. The cleared sections were imaged via confocal microscopy for 3D reconstruction of labeled structures.

Quantifications of astrocyte activation, perivascular macrophages, and resident macrophages were carried out using Fiji/Image[12]. Brain slices from five mice at each time point (SHAM and D28) were imaged, with five

tiles in the parietal region analyzed per mouse. Images were acquired under consistent parameters, including laser power, exposure, pinhole size, and image dimensions. A Z projection was applied to 3D stacks for 2D representation. An automatic threshold was employed to segment activated astrocytes and resident macrophages from the background, using identical settings across all samples. For each mouse, the mean value of the five tiles was used to quantify the areas of astrocyte activation (GFAP staining) and resident macrophages (IBA1 staining). Perivascular macrophages coverage wasquantified by two blind readers, who divided the number of labeled macrophages by the vessel length (µm) according to CD206 staining.

Heart assessment

- **Echocardiography**

Left ventricular (LV) ejection fraction and dimensions were measured on a high-resolution echocardiography (VEVO 2100, VisualSonics Inc., Toronto, Canada) with a 30 MHz transducer[13]. Mice were anesthetized using 1,5% oxygenated isoflurane by inhalation and were anchored to a warming platform in a supine position and prepared to minimize ultrasound attenuation. Uni'gel ECG (Asept Inmed, France) was applied to the thorax for optimal imaging. The ejection fraction was evaluated by planimetry as recommended[14]. Two-dimensional, long- and short-axis views were acquired to determine end-systolic (ESV) and end-diastolic (EDV) volumes using a cylindrical-hemi ellipsoid model. LV ejection fraction was calculated as: (EDV-ESV)/EDV x 100. The cardiac wall thickness (left ventricular posterior wall (LVPW), interventricular septum (IVS), and left ventricular internal diameter (LVID) were calculated by tracing wall limits in both the long and short axis views. LV-mass was corrected for body weight and expressed as LV-mass-index (LVMass) (mg/g)[15].

Kidney assessment

- **Blood and urinary tests**

Blood samples were collected in heparinized tubes. After centrifugation (2,500 x g for 10 minutes), plasma creatinine and blood urea nitrogen (BUN) were measured using an enzymatic method (Architect C16000, Abbott Diagnostics, Rungis, France). Urinary creatinine (UCr) was measured using the same enzymatic method. Albuminuria was evaluated using the Mouse Albumin ELISA Kit (Crystal Chem, IL, USA; Cat# 80970), following the manufacturer's instructions.

- **Electron microscopy**

Animals were anesthetized. An anterior thoracoabdominal incision was performed, and the heart, brain, and kidneys were immediately immersed in cold 1X PBS, stopping the heartbeat. The left ventricle, the brain, and the kidney were then carefully sliced under an optical magnifier and fixed in 4% PFA/2% glutaraldehyde (#16220, Euromedex, France) at 4°C. Kidney sections were post-fixed at room temperature (RT) in 1% osmium tetroxide in the dark and dehydrated with a graded ethanol series. A final dehydration step is performed with acetone and embedded in Epon. Ultrafine sections of 70 nm thick were then collected on copper grids (Electron Microscopy Sciences, Hatfield, PA, USA) and observed with a transmission electron microscope Hitachi H7650 (Hitachi High Technologies, Tokyo, Japan).

- **qPCR and podocin staining**

Gene expression analysis was performed on kidney samples (6 mice per group) from 129/Sv mice under SHAM and AngII conditions at day 28 using RT-qPCR. Total RNA from kidney mouse tissue was isolated by using the Direct-zol™ RNA MicroPrep kit (R2062, Zymo Research) and reverse transcribed into cDNA using the M-MLV Reverse Transcriptase (Promega). Quantitative real-time PCR was performed using the GoTaq qPCR master mix (Promega) on a QuantStudio™ 3 qPCR System (Thermo Fisher Scientific, MA, USA). Expression levels of key genes involved in podocyte and endothelial functions (*Nphs1*, *Nphs2*, *Thsd7a*, *NPR3*, *Wt1*, and *Flt1*)

were normalized to cyclophilin A and compared between conditions (Supplementary data, Table S1).

Immunofluorescence staining was conducted to visualize glomerular structures in C57BL/6J and 129/Sv mice under SHAM and AngII conditions. Podocin (NPHS2) staining was performed using the anti-Podocin polyclonal antibody (PA5-79757, Thermo Fisher Scientific, MA, USA).

Retinal assessment

- **Retinal vasculatures analysis**

Mice were intravenously injected with 75 µl of dextran (D3328, Texas Red™, 3000 MW, Lysine Fixable, ThermoFisher Scientific, MA, USA). Twenty minutes later, eyes were collected and fixed in 4% PFA for 30 minutes. Immunostaining on the whole-mount retina was conducted as previously described[16]. Retinas were stained with conjugated isolectin-B4-FITC (L2895, Sigma-Aldrich, MO, USA, dilution 1:200) diluted in PBS-1% Donkey serum (D9663-10ML, Sigma Aldrich, MO, USA) for 2 hours at room temperature before being flat mounted with Fluoromount G mounting medium (00-4958-02, ThermoFisher Scientific, MA, USA). Retinal vasculatures were imaged and analyzed with a fluorescent Axio Observer microscope (Zeiss, Germany). Dextran extravasation was assessed on retinal whole-mounts using a binary scoring approach (present/absent) based on the identification of focal TMR-positive spots outside the IB4-labelled vasculature on high-magnification images.

- **Blood-retina barrier analysis**

Retinas were promptly removed just after death, fixed overnight in 4% PFA – 1X PBS solution at 4 °C, and cryoprotected in successive sucrose solutions (10%, 20%, and 30%) diluted in 1X PBS before being stored at −80 °C. Transverse retina sections (14 µm thickness) were cut using a Microm HM550 cryostat (Microm, Walldorf, Germany) at −20 °C. The sections were mounted onto Polysine® glass slides (Polysine® Adhesion slides, Thermo Scientific, MA, USA) and stored at −80 °C until further processing. For staining, nonspecific binding sites were blocked with 10%

normal horse serum and 0.5% Triton X-100 in PBS for 1 hour at room temperature (RT). The sections were incubated with primary antibodies overnight (CRALBP 1/500, sc-48354Santa Cruz, France; lectin DyLight649, L32472, ThermoFisher Scientific, MA, USA). After washing with 1X PBS (three times for 10 minutes at RT), sections were incubated for 1 hour at RT with the appropriate secondary antibodies (donkey anti-mouse) conjugated to Alexa Fluor 488 (diluted 1/500, Invitrogen, France). Following washing, sections were mounted with a fluorescent aqueous mounting medium containing DAPI. Images were acquired with a confocal microscope (LSM 700, Carl Zeiss) using a 20× objective at 1024 × 1024 pixels resolution. All immunostaining experiments were repeated three to five times with different animals.

Female mice

Female 129S1/SvImJ mice were included in the study and underwent the same housing conditions, surgical procedures, angiotensin II (600 ng/kg/min for 28 days) or saline infusion, and postoperative monitoring as male mice. Blood pressure measurements and organ-specific analyses were performed using identical protocols. Cognitive testing was performed in male mice only, to limit animal numbers and in accordance with the study design.

Tissue Collection, Fixation, and Histological Analysis

Mice were anesthetized with ketamine (250 mg/kg, i.p.) and xylazine (20 mg/kg, i.p.). Transcardiac perfusion was performed by inserting a blunted butterfly needle into the left ventricle after cutting the right atrium. For heart immunohistochemical analysis, whole hearts were arrested in diastole using 1 mol/L potassium chloride. PBS was perfused at a rate of 2 mL/min, followed by 4% PFA. The heart, kidneys, and brain were excised and post-fixed in 4% PFA at 4°C overnight before being embedded in paraffin. Seven µm paraffin heart sections were stained with wheat germ agglutinin (WGA) and DAPI. The diameter of cardiomyocytes was measured in high-magnification (40×) images from five randomly selected

areas in five mice, analyzing 50 cells per mouse (250 cells per group). Picrosirius Red staining involved immersing tissue sections in a 0.1% Sirius Red solution in saturated picric acid for one hour, followed by washing in distilled water, dehydrating in absolute alcohol, clearing in xylene, and coverslipping[17]. Sagittal hemibrain slices were cut every 100 µm and stained with Pearls' Prussian blue to detect microbleeds larger than 50 μm^2, and hemalum-eosin to identify ischemic areas[18]. Following standard histological protocols, the kidney sections were stained with Periodic Acid–Schiff (PAS) to highlight glomerular and tubular basement membranes.

RNA extraction

On day 7 and day 28 after pump insertion, mice were euthanized by cervical dislocation. As previously described[19], microvessels isolation was performed using 6 mice per group. All procedures were carried out in a cold environment to minimize cell activation. Ipsilateral cortices were homogenized in MCDB131 medium (ThermoFisher Scientific, 10372019, MA, USA) containing 0.5% fatty acid-free BSA (Sigma Aldrich, 126609, MO, USA). The homogenate was centrifuged at 2,000 g for 5 minutes at 4°C. The resulting pellet was suspended in 15% dextran (~70 kDa, MilliporeSigma, 31390, MA, USA) in PBS and centrifuged at 10,000 g for 15 minutes at 4°C. The microvessels pellet was resuspended in MCDB131 with 0.5% fatty acid-free BSA and centrifuged at 2,000 g for 10 minutes at 4°C. RNA was extracted from cerebral-enriched microvessels (6 mice per group) using QIAzol lysis reagent (3722047, Qiagen, Germany) and the Qiagen RNeasy Mini Kit (Qiagen, Germany) as previously described. RNA purity was determined for RNA sequencing by assaying 1,5 µl of total RNA prep on a NanoDrop 8000 spectrophotometer.

Bulk RNA-sequencing

Total RNA integrity was checked using an Agilent Technologies 2100 Bioanalyzer with an RNA Integrity Number value (PCRq'UB platform, Bordeaux University). RNA sequencing bundle with PolyA was performed by Genewiz (Azenta Life Sciences, South Plainfield, NJ, USA). RNA library

preparation was prepared following the manufacturer's recommendations (KAPA mRNA HyperPrep Kit from ROCHE). Final samples from the pooled library prep were sequenced on Nextseq 500 ILLUMINA, 2x150bp corresponding to 30 million paired end reads per sample. The quality of raw data was evaluated with FastQC. Genetic and isoform abundances were quantified with rsem 1.2.28, before normalization with edgeR Bioconductor package[20]. Finally, differential analysis was conducted using the glam framework likelihood ratio test from edgeR. Multiple hypothesis-adjusted p-values were calculated using the Benjamini—Hochberg procedure to control FDR. Mammalian Phenotype Ontology (MPO) enrichment analysis was performed to identify phenotypic associations of differentially expressed genes (DEGs) and provide a functional interpretation of transcriptional changes. By linking gene expression to defined phenotypic traits, MPO allows for a more biologically relevant analysis of disease mechanisms. Gene enrichment was conducted using the MouseMine platform (https://www.mousemine.org), enabling the systematic identification of overrepresented phenotypic terms associated with the observed transcriptional alterations.

Statistical Analysis

Data were expressed as mean and standard deviation (SD) for normally distributed data or median and interquartile range (IQR) for non-normally distributed data. Parametric (unpaired t-test) or non-parametric (Mann-Whitney U test) tests were selected based on the data distribution for comparisons between the two groups. For multiple group comparisons, statistical analyses were performed using one-way ANOVA or repeated measures ANOVA, depending on the data structure. A two-way ANOVA was conducted to evaluate the main effects and interactions between factors for experiments with two independent variables (group and time). Post-hoc comparisons, such as Bonferroni or Tukey's tests, were applied to identify specific group differences following significant ANOVA results. All p-values were two-tailed, with statistical significance defined as $p < 0.05$. The sample size, what each n represents, the statistical tests used, and the

result are indicated in each figure legend. Statistical analyses were performed using RStudio Statistical Software (v. 2024.09.1+394; Posit Software, PBC, Boston, MA) for transcriptomic analysis and GraphPad Prism 10 (GraphPad Software, Inc) for other analyses.

III. Results

C57BL/6J and 129/Sv display the same blood pressure elevation upon AngII exposure

To induce hypertension, we chose angiotensin II (AngII) infusion, a widely validated experimental model known to reliably produce moderate and stable elevation in blood pressure, closely mimicking human hypertension, and allowing controlled investigation of associated organ-specific complications.

129/Sv and C57BL/6J mice were implanted with an osmotic pump delivering 600ng/kg/min of AngII (AngII group) or a saline solution (SHAM group) (Figure 1A). At baseline, sBP was 105.9 ± 7.9 in the C57BL/6J strain and 110.7 ± 8.9 mmHg in the 129/Sv strain (p = 0.32). Under AngII infusion, sBP rose significantly and remained stable in both strains at day 7, day 14, and day 21 (two-way ANOVA, p = 0.090 for weeks and p=0,14 for strains) (Figure 1B) with no significant difference at any time point (e.g., 141.5 ± 6 mmHg in C57BL/6J vs. 143.4 ± 11.8 mmHg in 129/Sv at day 7; p = 0.510). In a subset of animals with available telemetry at day 28 (n = 4 per AngII group), systolic blood pressure was comparable to earlier time points and did not differ between strains (Supplementary Figure S1). Systolic, diastolic, mean arterial pressures, and heart rate were similar between strains at all telemetry time points under angiotensin II infusion, including at day 28 (Supplementary Table S1). Representative telemetry traces illustrating blood pressure and activity patterns are shown in Supplementary Figure S2.

At day 28, all mice were alive and their weights were similar between the two groups (28.5 ± 3.4 g for C57BL/6J vs 28.3 ± 3.3 g for 129/Sv; p = 0.85).

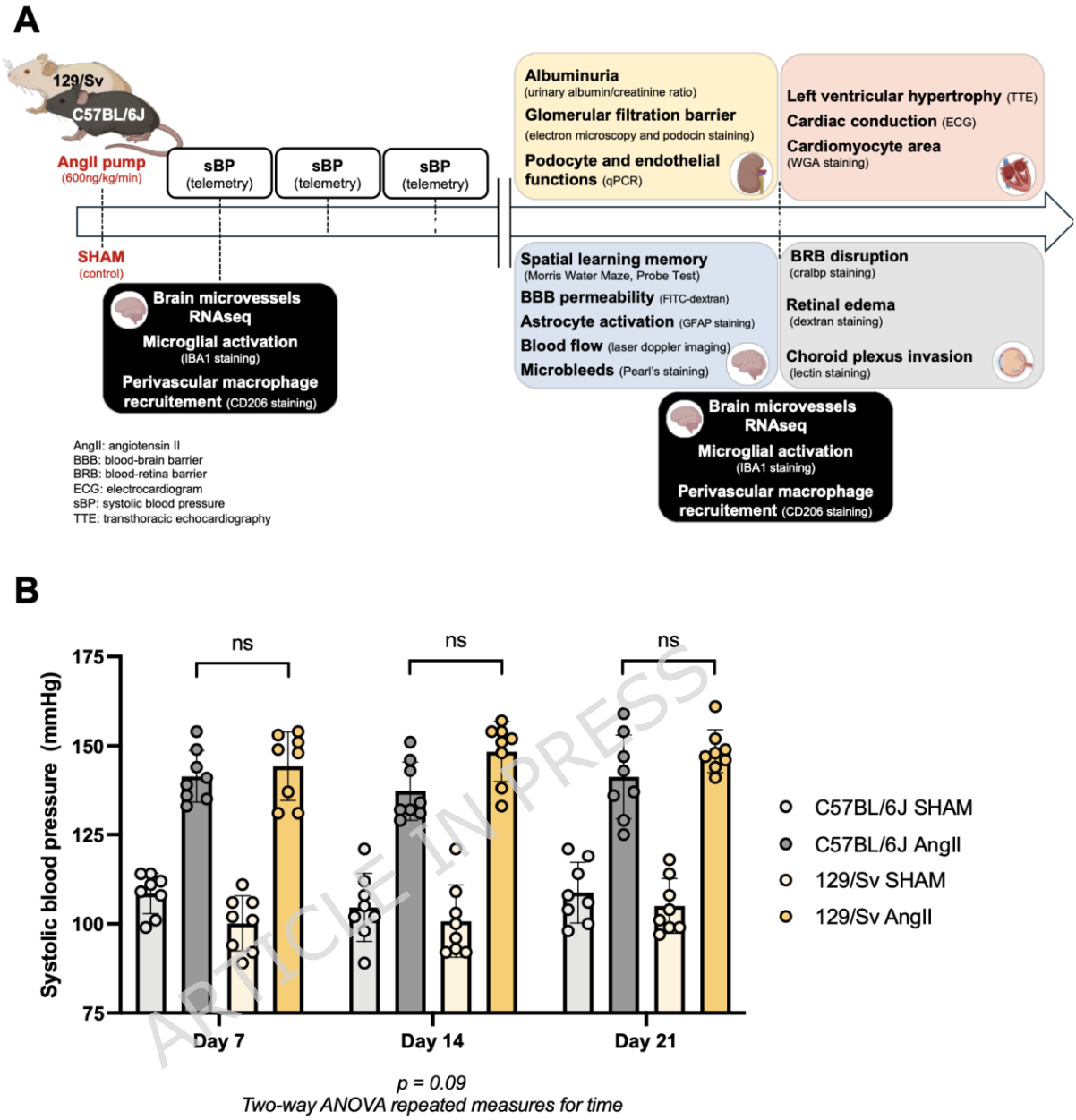

Figure 1. Experimental timeline and systolic blood pressure in 129/Sv and C57BL/6J mice after saline 0.9% (SHAM) or AngII infusion

(A) Schematic representation of the experimental timeline. AngII (600 ng/kg/min) or saline (SHAM) was infused via osmotic minipumps from day 0 (D0) in 129/Sv and C57BL/6J strains. Systolic blood pressure (sBP) was measured weekly using invasive telemetry. At D28, the four target organs of hypertension (brain, heart, kidney, and retina) were evaluated through various analyses. Transcriptomic analyses were performed at D7 and D28.

(B) sBP was measured with invasive telemetry at D7, D14, and D21 across four groups of mice (C57BL/6J SHAM, C57BL/6J with AngII, 129/Sv SHAM, and 129/Sv with AngII). Under AngII treatment, the 129/Sv and C57BL/6J mouse strains show increased sBP. However, as a two-way ANOVA ($p = 0.09$) indicates, this elevation does not significantly vary over time between the two strains.

Only hypertensive 129/Sv mice exhibit cognitive impairment, blood-brain barrier disruption, microbleeds, and astrocyte activation

In humans, hypertensive brain injury often manifests as cerebral small vessel disease (cSVD), characterized by cognitive impairment leading to vascular dementia. A central pathological feature of cSVD is disruption of the blood-brain barrier (BBB). We therefore examined cognitive functions, BBB integrity, and related cerebral lesions in hypertensive mice to assess strain-specific vulnerabilities and recapitulate human disease patterns.

In hypertensive C57BL/6J and 129/Sv mice, cognitive functions, particularly hippocampal memory integration, were tested using the Morris Water Maze starting at day 21. Visual acuity was assessed before the Morris Water Maze using the visual cliff test, confirming that no mice exhibited visual impairments. In the Morris Water Maze, no significant differences in latency or velocity were observed between SHAM and AngII-treated mice in the pre-training phase, indicating unaffected locomotor activity and learning performance (Supplementary data, Figure S1). After 21 days of AngII treatment, the 129/Sv AngII group demonstrated significant deficits in spatial learning and memory compared to 129/Sv SHAM, highlighting marked cognitive impairments in this strain. In the 129/sv strain, both groups performed similarly on day 1. Only 129/Sv SHAM mice showed improvement over time ($p = 0.0008$) (Figure 2A). Conversely, no significant cognitive impairment was observed in C57BL/6J AngII mice compared to SHAM, which showed similar performance in MWM ($p = 0.18$) (Figure 2B). In the Probe test (28 days after treatment (AngII or saline)), 129/Sv SHAM mice had significantly lower proximity measures than 129/Sv AngII ($p = 0.047$) (Supplementary data, Figure S2).

CBF has been described as altered in vascular cognitive impairment[21]. We measured CBF before sacrifice (28 days of AngII). In both strains, AngII led to a reduction in brain CBF, but this decrease was

similar between groups (1097 ± 131.6 AU in C57BL/6J vs 1124 ± 112.3 AU in 129/Sv; p = 0.700) (Figure 2C).

An increased brain-blood barrier (BBB) permeability was identified as one of the earlier BBB dysfunctions in the context of aggression[22]. We evaluated BBB permeability after 28 days of AngII or saline in both strains, using a 3kDa fluorescent dextran injected 20 minutes before the sacrifice. Results were expressed as the permeability index (PI) ratio of the AngII group relative to the SHAM group in each strain. After AngII infusion, the PI ratio was 1.33 ± 0.15 vs. 1.9 ± 0.30 (p = 0.006) in C57BL/6J vs 129/Sv, respectively (Figure 2D), showing a significant increase in BBB permeability in 129/Sv strain as compared to C57BL/6J. We did not find any vascular extravasation of larger molecules, including IgG (150 kDa) and fibrinogen (340 kDa), in immunostaining of brain paraffin slices (n = 5) (data not shown).

Cerebral lesions associated with hypertension are mostly small vessel lesions characterized by microinfarction and microbleeds[23]. Microbleeds were significantly more frequent in the 129/Sv AngII group than in the C57BL/6J AngII group (3 [2-4.75] vs. 1 [0.25-1.50]; p = 0.016) (Figure 2E). However, we did not find any ischemic areas in any group or strain (data not shown).

GFAP staining is a reliable marker for astrocyte activation, which can be induced by increased BBB permeability[24]. In the 129/Sv strain, a significant increase in GFAP staining was found after AngII infusion compared to C57BL/6J. In the hippocampal area, the mean GFAP surface area in the 129/Sv strain was 5.77 ± 0.59 % in SHAM condition and 7.47 ± 1.10 % after 28 days of AngII (p = 0.042) (Figure 2F).

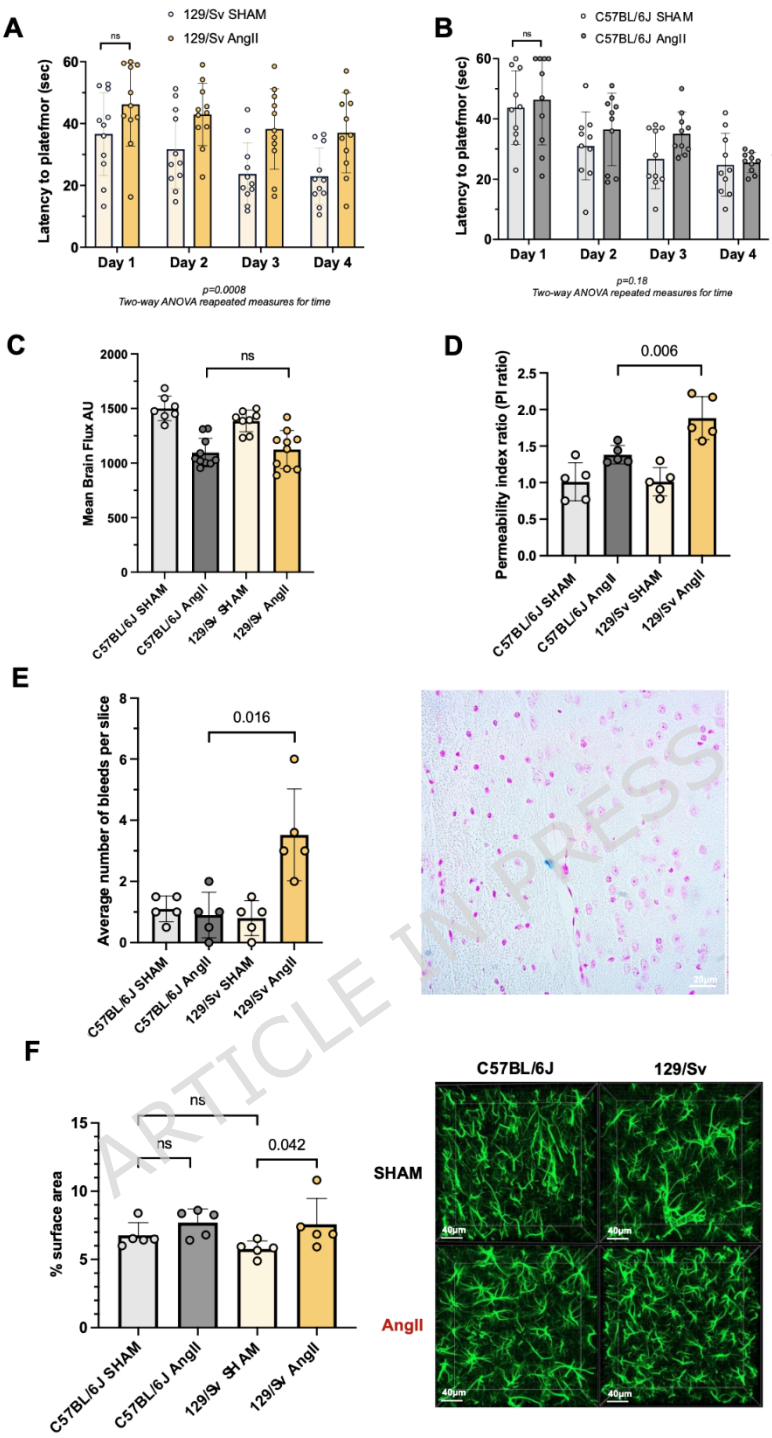

Figure 2. Brain effect of AngII infusion in both strains.

(A) and (B) Morris Water Maze test showed similar spatial learning and memory in C57BL/6J mice under AngII compared to SHAM, but a disability in 129/Sv mice under AngII compared to their respective SHAMs. Graph shows the latency to reach the hidden platform (expressed in seconds) over 4 training days. Two-way ANOVA with repeated measures for time.

(C) Mean brain CBF was similar in both AngII groups (1097 ± 131.6 AU in C57BL/6J vs 1124 ± 112.3 AU in 129/Sv; p = 0.70)

(D) A significant increase in blood-brain barrier permeability was only found in 129/Sv mice after AngII infusion (permeability index ratio with 3kDa dextran)

(E) Illustrative Pearl's staining image of the brain from 129/Sv hypertensive mice. Using a systematic analysis of slices every 100 μm with Pearl's staining, we found an increased average of microbleeds only in 129/Sv mice after AngII infusion (microbleeds larger than 50 μm2).
(F) Representative immunofluorescence image of hippocampus area from both strains under two conditions. 129/Sv mice expose an astrocyte activation profile in hippocampal area (GFAP staining) after AngII infusion

Only hypertensive 129/Sv mice develop severe albuminuria and podocyte injury without nephroangiosclerosis

In humans, hypertensive kidney injury commonly manifests as hypertensive nephropathy, often characterized by low grade albuminuria. We therefore assessed renal function, albuminuria, and podocyte integrity in hypertensive mice to determine whether strain-specific susceptibilities mirror these clinically relevant patterns.

Renal function assessed by plasma creatinine dosage and blood urea nitrogen (BUN) was comparable in both strains in the SHAM group and remained unaffected in the AngII group.

In C57BL/6J mice, the urinary albumin/creatinine ratio (UACR) remained low and stable following AngII infusion (SHAM: 5.5 ± 8.1 mg/mmol; D28: 12.5 ± 5.3 mg/mmol). By contrast, 129/Sv mice exhibited a dramatic increase in UACR at D28 (214.7 ± 90.8 mg/mmol) compared to their SHAM counterparts (8.2 ± 4.8 mg/mmol; $p = 0.0079$) (Figure 3A).

Given the previously described link between podocyte alteration and albuminuria[25], we assessed podocyte morphology using electron microscopy. Notable abnormalities, including flattening of podocyte feet and changes in the slit diaphragm, were observed after 28 days of AngII infusion in 129/Sv mice but not in C57BL/6J mice (Figure 3B). Immunofluorescence staining using the anti-Podocin antibody revealed a disruption of the continuous linear pattern observed in SHAM mice, with a shift towards a more granular and fragmented distribution in 129/Sv AngII-treated mice, suggesting strain-specific differences in podocyte integrity and glomerular structure (Figure 3C).

RT-qPCR analysis revealed significant downregulation of Nphs1 (podocyte filtration), NPR3 (sodium regulation), Wt1 (podocyte development), and Flt1 (vascular permeability) in 129/Sv mice under AngII compared to SHAM ($p < 0.05$), confirming impaired podocyte and endothelial functions (Figure 3D).

Other vascular lesions, including ischemic glomerulus and fibrosis, were systematically searched using periodic acid Schiff staining. For either

strain, no evidence of nephroangiosclerosis was identified in the AngII group (Supplementary data, Figure S3).

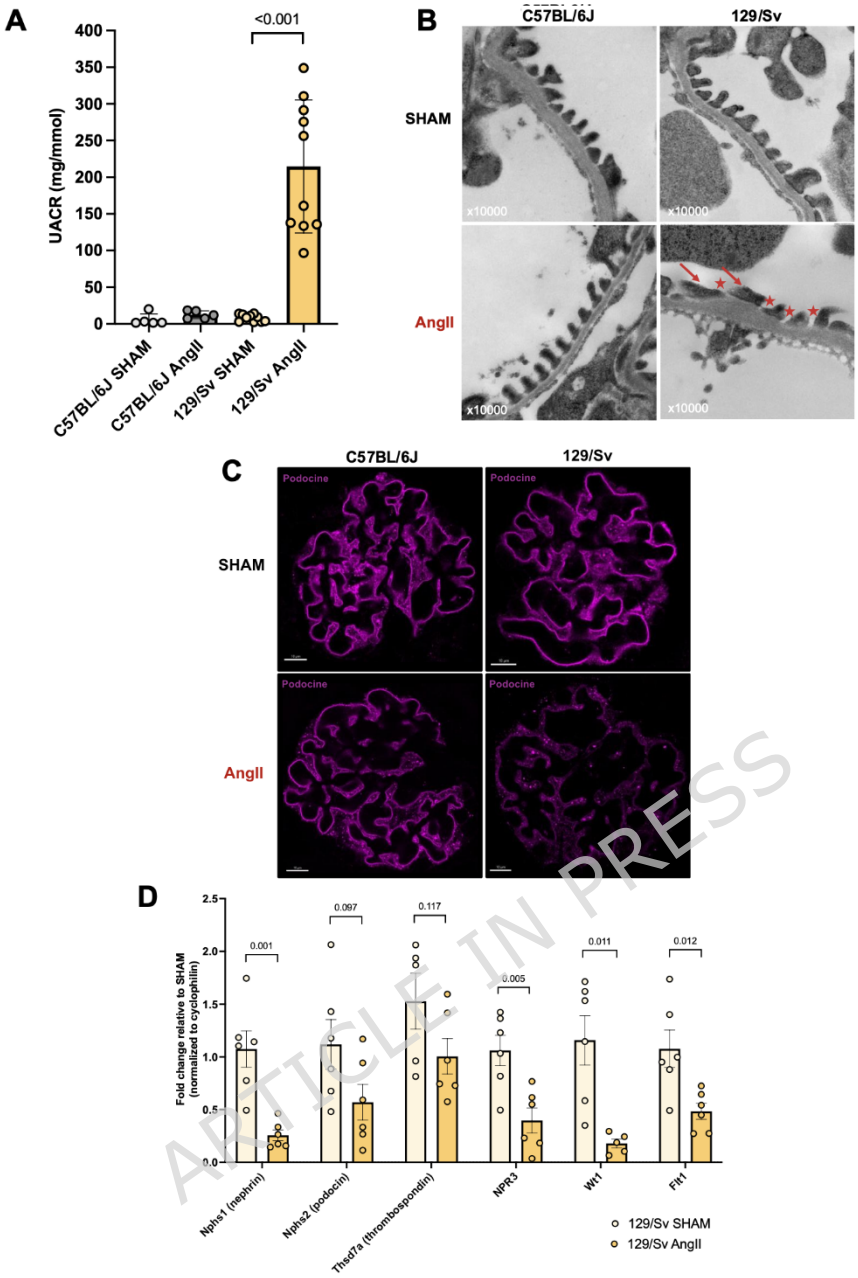

Figure 3. Kidney effect of AngII infusion in both strains.
(A) 129/Sv mice exhibited a significant increase urinary albumin/creatinine ratio (UACR) at D28 (214.7 ± 90.7 mg/g) compared to the SHAM group (12.5 ± 5.3 mg/g, $p < 0.001$)
(B) Representative electron microscopy image of the kidney from both strains under two conditions. After 28 days of AngII infusion, abnormalities in podocyte foot processes (red arrow) and the slit diaphragm (red star) are observed in 129/Sv mice compared to C57BL/6J.
(C) Representative immunofluorescence image of a glomerulus from both strains under two conditions. Podocin staining: continuous linear staining in C57BL/6J with AngII vs. granular pattern staining in 129/Sv with AngII
(D) qPCR of total kidney: decreased expression of podocyte and endothelial markers in 129/Sv strain after AngII. See Supplementary Table for the list of primers.

Only hypertensive 129/Sv mice exhibit hypertensive cardiopathy

The cardiac consequences of hypertension are dominated by left ventricular hypertrophy and fibrosis. To evaluate these effects, echocardiography was conducted on both mouse strains following the initiation of AngII or saline infusion. After 28 days of AngII treatment, the 129/Sv mice showed signs of hypertrophic cardiomyopathy, as evidenced by a significantly increased LVMass index (6.92 ± 0.96 mg/g vs. 5.17 ± 0.58 mg/g at baseline; $p = 0.005$), while no notable changes were found in the C57BL/6J strain (6.01 ± 0.65 mg/g vs. 6.15 ± 0.94 mg/g at baseline; $p = 0.78$). In the 129/Sv AngII group, there was an increase in systolic and diastolic left ventricular posterior wall (LVPW) and interventricular septal (IVS) thickness, accompanied by a decrease in left ventricular internal diameter (LVID). Conversely, the C57BL/6J strain did not exhibit significant differences in these parameters under AngII treatment (Table 1).

In addition to structural changes, hypertensive 129/Sv mice exhibit cardiac conduction disturbances evidenced by a prolonged QRS duration (Figure 4A).

To further investigate myocardial remodeling, picrosirius red staining was used to evaluate cardiac fibrosis. Following AngII infusion, no fibrosis was detected in the cardiac tissue of either strain (data not shown).

Cardiomyocyte hypertrophy was evaluated using wheat germ agglutinin (WGA) FITC immunostaining. After 28 days of AngII treatment, 129/Sv mice had a significantly larger cardiomyocyte cross-sectional area than C57BL/6J mice (113.04 ± 17 vs. 72.22 ± 7 μm^2; $p = 0.03$). However, no differences in cardiomyocyte cross-sectional area were noted between C57BL/6J and 129/Sv mice in the SHAM group (Figure 4B).

Table 1 : Echocardiography

	C57BL6/J (*n* = 10)			129/Sv (*n* = 10)		
	D0	**D28**	**p-value**	**D0**	**D28**	**p-value**
IVSd (mm)	0.96 (0.09)	1.06 (0.09)	0.37	0.92 (0.10)	1.31 (0.23)	**<0.001**
IVSs (mm)	1.28 (0.12)	1.40 (0.10)	0.38	1.21 (0.14)	1.76 (0.22)	**<0.001**
LVIDd (mm)	3.87 (0.46)	3.60 (0.54)	0.22	3.48 (0.33)	3.09 (0.35)	**0.04**
LVIDs (mm)	2.89 (0.52)	2.65 (0.58)	0.15	2.49 (0.31)	2.08 (0.44)	**0.02**
LVPWd (mm)	1.13 (0.20)	1.25 (0.22)	0.11	1.04 (0.13)	1.46 (0.17)	**<0.001**
LVPWs (mm)	1.41 (0.17)	1.50 (0.18)	0.06	1.23 (0.12)	1.83 (0.17)	**<0.001**
EF (%)	50.0 (12.90)	52.2 (13.00)	0.39	56.2 (6.94)	62.4 (11.00)	0.10
FS (%)	25.4 (8.40)	26.4 (9.05)	0.14	28.7 (4.69)	33.1 (8.16)	0.11
LVMass-index (mg/g)	6.01 (0.65)	6.15 (0.94)	0.78	5.17 (0.58)	6.92 (0.96)	**0.005**

EF: ejection fraction; FS: fractional shortening; IVSd: interventricular septal thickness in diastole; IVSs : interventricular septal thickness in systole; LVIDd: left ventricular internal diameter in diastole; LVIDs: left ventricular internal diameter in systole; LVMass-index: left ventricular mass index; LVPWd: left ventricular posterior wall thickness in diastole; LVPWs: left ventricular posterior wall thickness in systole

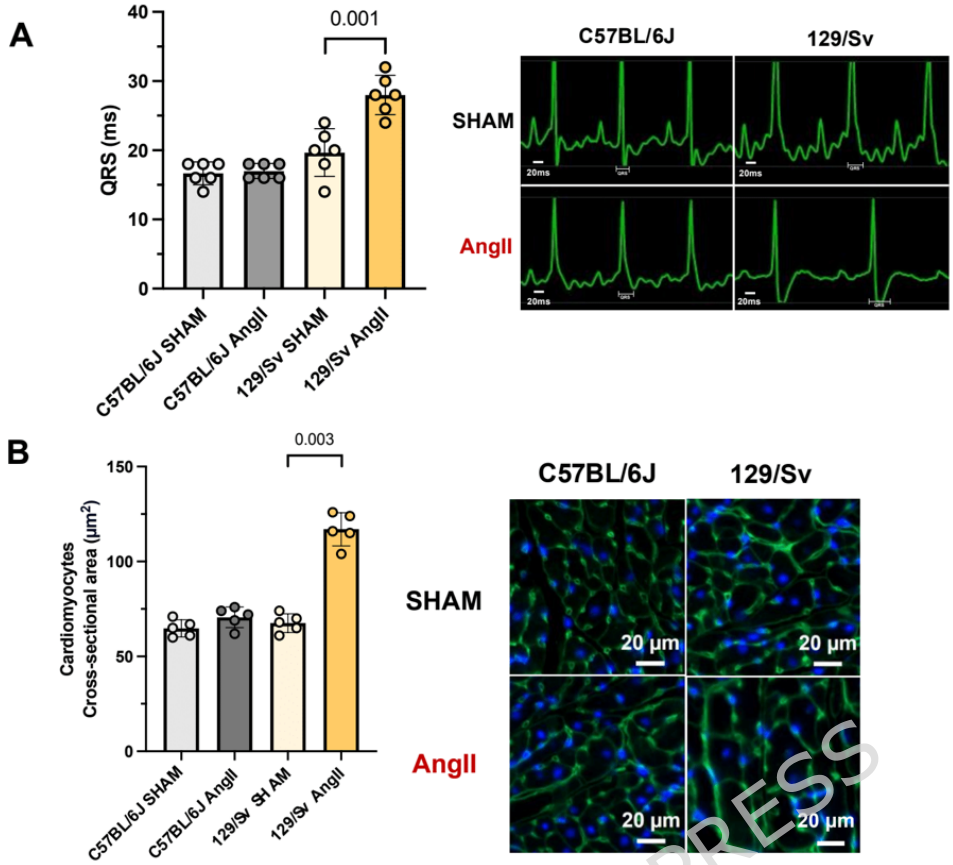

Figure 4. Heart effect of AngIIinfusion in both strains.
(A) Illustrative electrocardiogram from both strains under two condition. Hypertensive 129/Sv mice exhibit cardiac conduction disturbances with prolonged QRS duration.
(B) Representative immunofluorescence image of heart from both strains under two conditions. Significant increase in cardiomyocyte cross sectionala rea (WGAstaining) after 28 days of AngII infusion in 129/Sv vs. C57BL/6J strain (117.0 ± 8.7 vs. 67.6 ± 5.0µm2 ;p=0.03).

Only hypertensive 129/Sv mice develop blood-retinal barrier disruption

Hypertension can lead to various retinal complications, including hemorrhage, cotton wool spots, exudates, and papilledema in humans.

At day 28, a disruption of the blood-retinal barrier was observed in hypertensive 129/Sv mice, as evidenced by cellular retinaldehyde-binding protein (CRALBP) immunostaining and choroid plexus invasion revealed by lectin staining. Notably, these changes were absent in hypertensive C57BL/6J mice (Figure 5A).

We used TMR dextran three kDA lysine fixable as a tracer to further investigate retinal edema, a severe hallmark lesion. After 28 days of AngII

treatment, we observed vascular extravasation of the dextran in all retinas analyzed from 129/Sv mice. In contrast, no extravasation was detected in the retinas of C57BL/6J mice (Figure 5B and C).

The retinal lesions developed in 129/sv mice did not alter their visual acuity, measured by cliff test (data not shown).

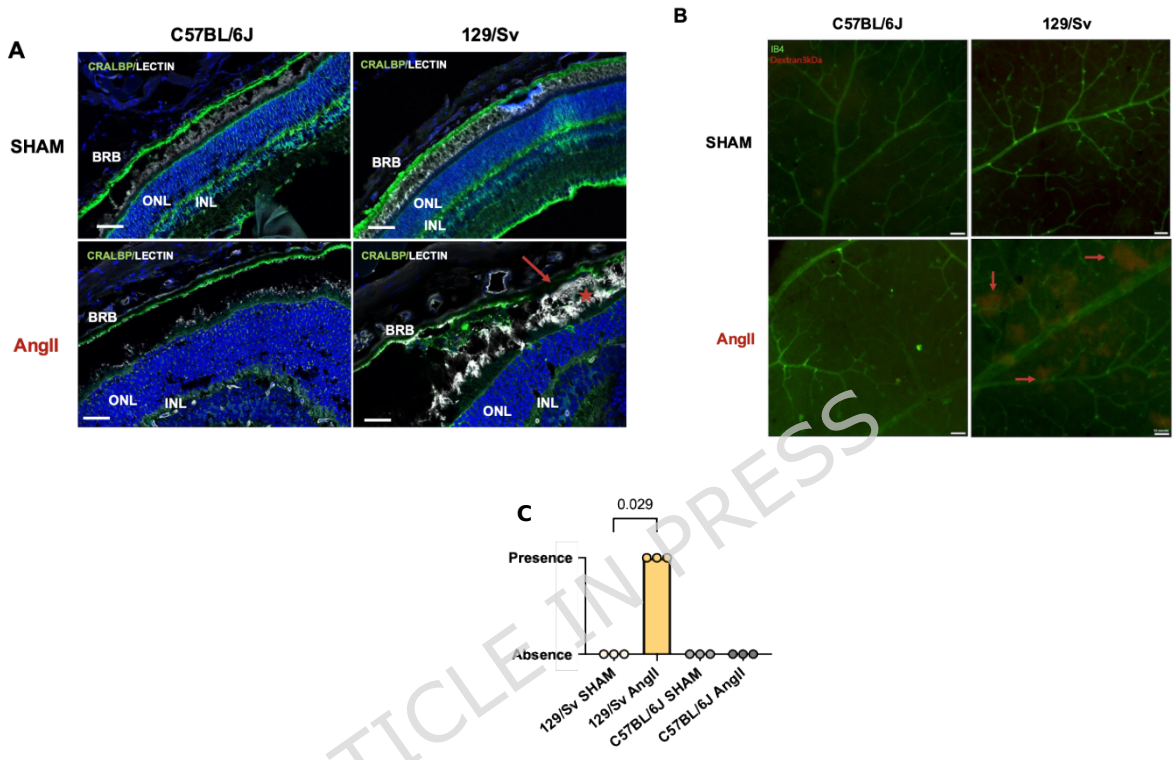

Figure 5. Retina effect of AngII infusion in both strains.
(A) Representative immunofluorescence image of the retina from both strains under two conditions. Blood-retina barrier disruption (red arrow) was observed in 129/Sv mice with AngII-induced hypertension, along with choroid plexus invasion (red star), whereas no such disruption was seen in C57BL/6J mice with AngII.
(B) After 28 days of AngII infusion, we found extravasation of dextran 3kDa (red arrow) on 129/Sv analyzed retinas (n=5) but none in C57BL/6J.
(C) Strain-dependent microvascular leakage induced by angiotensin II. Each dot represents one analysed image (each image, taken from different animals (n=3 mice per group, n = 3 per condition)). Focal extravasation of 3kDa dextran was scored as present or absent based on the presence of discrete perivascular TMR-positive spots. AngII induced focal microvascular leakage exclusively in 129/Sv mice, whereas no extravasation was observed in C57BL/6J mice or in SHAM-treated animals. Statistical comparison was performed using Fisher's exact test.
BRB: blood retina barrier; Ib4 : Isolectin Ib4 ; INL: inner nuclear layer ; ONL: outer nuclear layer

Female 129/Sv mice exhibit similar hypertensive organ damage as males upon 600 ng/kg/min AngII infusion

In the literature, a sexual dimorphism in the AngII-induced hypertension model is reported[26]. We decided to verify this hypothesis in a

cohort of female mice. Similar to the findings in male mice, three-month-old 129/Sv female mice treated by AngII experienced organ injuries. In female 129/Sv mice, no cognitive tests were performed, and only tissue lesions were assessed. Histologic analysis revealed increased astrocytic activation under AngII (GFAP staining), with no significant differences compared to male 129/Sv mice in the SHAM condition. We observed elevated UACR with AngII treatment in female 129/Sv mice, with no significant differences compared to male mice of the same strain. Lastly, female 129/Sv mice developed hypertrophic cardiomyopathy under AngII infusion, as did male mice (Supplementary data, Figure S4).

Transcriptomic analysis identifies strain-specific immune and vascular signatures associated with hypertensive complications

To better understand why 129/Sv mice developed severe organ damage while C57BL/6J mice remained protected despite similar hypertension levels, we conducted transcriptomic analyses on brain-enriched microvessels isolated from both strains. We focused specifically on cerebral microvessels for this transcriptomic analysis because the brain exhibited the most striking and clinically relevant phenotype among the target organs, and cerebral microvascular injury represents a hallmark of hypertensive cerebrovascular disease in humans, providing a robust proof-of-concept model to understand strain-specific susceptibilities. Comparisons between the strains were performed at two critical time points: day 7, to capture early transcriptomic responses preceding the appearance of irreversible tissue lesions, and day 28, representing chronic stages of hypertension with established end-organ lesions.

The volcano plots illustrate the differentially expressed genes (DEGs) between C57BL6/J and 129/Sv mice under AngII treatment at days 7 and 28 (Figure 6A).

To translate the observed gene-expression differences into meaningful biological insights, we performed a Mammalian Phenotype Ontology (MPO) enrichment analysis. The MPO database categorizes transcriptomic changes into known phenotypic consequences, facilitating interpretation of how differential gene expression could contribute mechanistically to observed organ-specific susceptibilities.

At day 7, comparison between strains revealed significant enrichment of immune-related and inflammatory MPO phenotypes, notably ‘abnormal immune system physiology’ (MP:0001790, $p < 0.0001$) and ‘abnormal inflammatory response’ (MP:0001845, $p < 0.0001$) in the 129/Sv strain compared to C57BL/6J (Figure 6B). These findings indicate an early and distinct activation of immune and inflammatory pathways in 129/Sv mice, whereas C57BL/6J showed a more limited transcriptional response. By day 28, enrichment patterns shifted towards cardiovascular and structural remodeling phenotypes, consistent with the transition from early molecular responses to established tissue injury in the 129/Sv strain. This temporal evolution highlights how strain background influences the dynamics of vascular and immune responses under hypertensive stress.

Specifically, genes associated with the MPO term “abnormal immune system physiology” (MP:0001790) were significantly upregulated in 129/Sv mice treated with AngII at day 7 compared to C57BL/6J mice (Figure 6C), further confirming the maladaptive early inflammatory response occurring uniquely in 129/Sv mice.

Detailed inspection of the differentially expressed genes within these immune-related categories revealed a prominent signature of interferon-stimulated genes (such as *Stat1*, *Irf7*, and *Ifit3*), suggesting that the interferon signaling pathway is a key component of this early molecular divergence.

These findings collectively indicate that genetic background modulates immune and vascular responses to hypertension, which are associated with differential susceptibility to cerebrovascular complications

Hypertensive C57BL/6J mice exhibit distinct microglial and perivascular macrophage recruitment in the brain

AngII was known to promote tissue inflammation cell recruitment[27], and inflammation was described as an actor of hypertension pathogenesis and complications[28]. In line with the transcriptomic analysis, we wish to validate this difference *in vivo* in the brain. IBA1 is a marker of microglia (resident macrophages in the brain), and IBA1 staining was used to assess inflammatory cell recruitment in the brain[29]. Perivascular macrophages (PVM) expressing CD206 in the brain play a crucial role in immune surveillance and maintaining homeostasis within the central nervous system[30].

After 28 days of AngII infusion, we found a significant increase in brain microglia staining using IBA1 staining in C57BL/6J in the hippocampal area compared with C57BL6/J SHAM mice (17.0 ± 2.0 % vs. 20.4 ± 1.9%; p=0.0263) (Figure 6D). Similarly, an increase in CD206 PVMs coverage was observed in the C57BL6/J strain under AngII with 1.13 ± 0.08 PVM/µm

vs. 1.34 ± 0.13 PVM/µm in C56BL6/J SHAM mice (p=0.0227) (Figure 6E). On the contrary, no difference was observed in IBA1 and CD206 staining in the 129/Sv strain under AngII (vs. SHAM procedure).

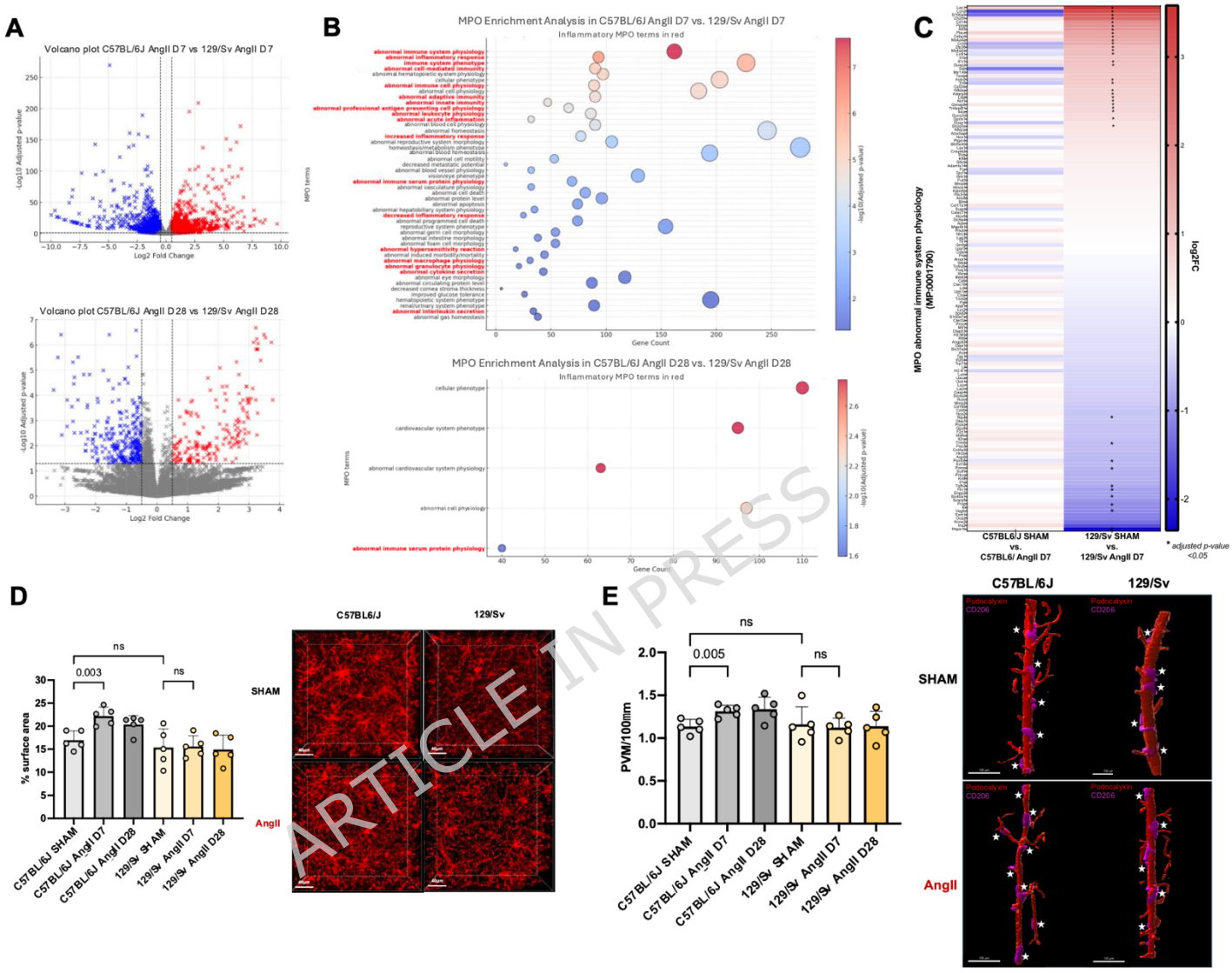

Figure 6. Transcriptomic and vascular differences between C57BL/6J and 129/Sv mice under AngII treatment

(A) RNA-sequencing was performed on brain-enriched microvessel preparations from both strains under two conditions to investigate the biological processes underlying strain differences. Volcano plots illustrate the differentially expressed genes (DEGs), represented as $\log_2$ fold change (FC) vs. $-\log_{10}$ adjusted p-value, comparing C57BL/6J and 129/Sv mice under AngII at D7 (top) and D28 (bottom). Significant downregulated (log2FC <-1, in blue) and upregulated (log2FC >1, in red). In gray: non-significant genes.

(B) Mammalian Phenotype Ontology (MPO) enrichment analysis of differentially expressed genes between C57BL/6J and 129/Sv mice under AngII at D7 (B) and D28 (C). Dot size represents gene count, and color indicates statistical significance (-log10 adjusted p-value). The MPO terms highlighted in bold and red font correspond to phenotypes related to inflammation.

(C) Heatmap of differentially expressed genes between C57BL/6J and 129/Sv mice under AngII. The color scale represents log2 fold change, with red indicating upregulation (log2FC >1) and blue downregulation (log2FC <-1). Significant genes are marked with asterisks.

(D) Representative immunofluorescence image showing microglial activation in the hippocampal area from both strains under two conditions. Quantification of IBA1-positive microglial activation in

the hippocampal area. A significant increase in microglial activation is reported in C57BL/6J with AngII.
(E) Representative immunofluorescence image showing perivascular macrophage coverage in the brain from both strains under two conditions. Quantification of CD206-positive perivascular macrophages in the parietal cortex. A significant increase in CD206-positive macrophages is observed in C57BL/6J mice with AngII.

IV. Discussion

Hypertension is a major risk factor for cardiovascular and renal diseases, but the severity of organ damage varies widely among individuals. This variability suggests a strong genetic component influencing susceptibility to hypertensive complications. Our study emphasizes the critical influence of genetic background, showing that under a moderate-dose angiotensin II infusion in young adult mice, 129S1/SvImJ mice exhibit greater susceptibility to hypertensive target-organ damage, whereas C57BL/6J mice show relative protection in this experimental setting. These differences highlight the importance of considering strain background when modeling hypertensive complications.

Despite comparable hypertensive burden, 129/Sv mice exhibited widespread target organ damage, including cognitive impairment, BBB hyperpermeability, astrocyte activation, and increased microbleeds in the brain, along with retinal vascular permeability, hypertrophic cardiomyopathy, and podocyte injury-associated albuminuria in the kidneys. In contrast, C57BL/6J mice showed minimal or no such complications, reinforcing the hypothesis that genetic background dictates the severity of hypertension-related injury rather than the magnitude of BP elevation alone. The absence of overt LVH in C57BL/6J mice under moderate Ang II infusion is consistent with the dose- and context-dependence of Ang II–induced cardiac remodeling, supporting a strain-dependent rather than exposure-limited interpretation of the observed phenotypes.

The immune response to AngII differs fundamentally between strains. In C57BL/6J, in response to low-dose AngII infusion, we observe a low-grade, controlled inflammatory profile (characterized by microglial activation and perivascular macrophage recruitment), associated with preserved BBB integrity, and suggesting a strain-specific neurovascular phenotype[31].

Conversely, 129S1/SvlmJ mice showed early immune activation associated with BBB hyperpermeability and cognitive impairment. This pattern closely resembles those described in cerebral small vessel disease (cSVD) in humans [32,33]. In 129S1/SvlmJ, inflammatory signaling was more pronounced and sustained, paralleling greater neurovascular damage. These results underscore the importance of inflammatory and immune-mediated mechanisms in modulating hypertensive injury and offer a dependable preclinical model for examining the genetic determinants of hypertension-induced end-organ damage. Together, these findings highlight that 129S1/SvlmJ mice provide a robust model to study strain-dependent patterns of hypertensive target organ damage.

BBB dysfunction has been reported as a delayed consequence of endothelial injury, possibly driven by AngII-mediated oxidative stress, aldosterone, endothelin-1 signaling, or recruitment of inflammatory cells[34,35].

Glial cells play a fundamental role in maintaining neurovascular integrity and promoting neuroinflammatory tolerance[36]. Glial activation was associated with preserved neurovascular function in C57BL/6J mice, whereas in 129/Sv mice, the absence of this response contributes to greater susceptibility to hypertensive damage. Similar findings have been reported by Faraco *et al.*, who showed that AngII with salt-induced hypertension promotes perivascular macrophage recruitment and reactive oxygen species production, leading to BBB destabilization[7]. However, in C57BL/6J mice, this inflammatory response occurs without leading to BBB hyperpermeability, indicating a distinct pattern of immune activation across genetic backgrounds. These findings highlight a significant difference in how inflammatory pathways influence hypertensive outcomes across genetic backgrounds within the experimental context studied here.

We analyzed cerebral microvessel transcriptomes to characterize the molecular responses underlying these strain differences in susceptibility. By day 7 post-AngII, 129/Sv mice showed a marked upregulation of immune-related and endothelial stress pathways. In contrast, C57BL/6J mice exhibited a more limited transcriptional response, suggesting distinct

regulatory thresholds of vascular and immune activation between strains. By day 28, the transcriptomic profiles in 129/Sv mice shifted towards signatures of fibrosis and vascular remodeling, consistent with the progression from early molecular activation to established structural injury. In comparison, C57BL/6J mice maintained a stable transcriptional landscape over time. Together, these findings indicate that early molecular responses diverge substantially across genetic backgrounds and support the use of 129/Sv mice as a model for studying the progression from hypertension to overt target organ damage. Beyond MPO-level enrichment, the cerebral microvessel transcriptomic signature is hypothesis-generating and highlights candidate immune–endothelial programs for future functional studies. Among these, interferon-related signaling emerges as a plausible pathway to explore, without implying causality.

In contrast, 129/Sv mice exhibited a delayed and amplified immune activation, temporally associated with increased end-organ damage. The limited neuroinflammatory recruitment in this strain coincides with more extensive end-organ damage. This aligns with prior studies highlighting the role of immune cell activation in determining susceptibility to hypertensive injury[37,38]. These findings suggest that a distinct inflammatory profile are associated with differential susceptibility to hypertensive damage across genetic backgrounds, without establishing a direct causal role for immune activation.

This pattern was consistently observed in male and female mice, challenging the hypothesis that female mice are inherently shielded from AngII-induced hypertension[26]. The consistency of these findings across sexes strengthens the reliability of this hypertensive model.

We acknowledge that our standardized 1-hour recording protocol during the light phase does not capture nocturnal blood pressure or activity-related hemodynamic variability. However, resting blood pressure has been identified as a major determinant of hypertensive target organ damage, supporting the translational relevance of our monitoring window in assessing strain-specific vulnerabilities. Although a non-significant numerical trend toward higher systolic blood pressure was observed in

129S1/SvlmJ mice, the severity and multi-organ nature of the observed lesions appear highly disproportionate to this modest hemodynamic difference. While we cannot formally exclude that a lack of statistical power may mask subtle blood pressure variations, the massive divergence in phenotypes strongly supports a primary role for strain-specific genetic susceptibility rather than hemodynamic exposure alone.

Our study identifies the 129S1/SvlmJ strain as a relevant model for severe hypertensive complications under moderate AngII–induced hypertension in young adult mice, mirroring human lesions in cSVD, cardiac hypertrophy, and renal dysfunction, further underscoring its translational relevance. The model also provides an opportunity to investigate how immune and vascular pathways interact with genetic susceptibility in the development of hypertensive complications. Given the strain-specific differences observed in perivascular macrophage coverage and endothelial transcriptomic responses, interventions aimed at modulating neurovascular inflammation could be explored to enhance resilience in susceptible populations.

Finally, these findings reinforce the necessity of incorporating genetic background considerations into preclinical hypertension research. Many current hypertensive models rely predominantly on C57BL/6J mice, which, as demonstrated here, may underestimate the extent of end-organ damage observed in human pathology. Hamzaoui *et al.* reported that compared to C57BL/6J, the 129/Sv strain exhibits more severe cardiovascular injury following 5/6 nephrectomy, further supporting its utility in modeling hypertensive organ damage[10].

These findings provide a unique platform for dissecting the interplay between genetics and hypertension-induced organ damage. Moreover, they position the 129S1/SvlmJ strain as a critical model for studying hypertensive complications and developing targeted therapeutic interventions.

In conclusion, this study demonstrates that genetic background significantly influences the severity of hypertensive complications under a

moderate-dose angiotensin II infusion in young adult mice. Despite comparable blood pressure elevations, 129/Sv mice exhibited widespread end-organ damage, while the C57BL/6J strain remained relatively protected within this specific experimental setting. Our transcriptomic analysis highlights strain-specific inflammatory and endothelial responses, providing a mechanistic basis for these disparities. By identifying 129S1/SvlmJ as a highly susceptible strain to moderate hypertensive stress, we establish a robust and translational preclinical framework to study the genetic and molecular determinants of hypertension-induced organ damage.

Acknowledgments

We sincerely thank Béatrice JASPARD-VINASSA and Muriel BUSSON for scientific advice, Philippe ALZIEU, Sylvain GROLLEAU, Maxime DAVID for their technical assistance and animal care; Christelle BOULLE and Hélène AOUIZERATE for administrative assistance.

We thank Prof. Céline GUILBEAU-FRUGIER (UMR 1297, Toulouse, France) for Electron Microscopy images

This work benefited from equipment and services from the PCRq'UB platform (Bordeaux University).

We thank Fondation pour la Recherche Médicale (FRM) for it support)

Sources of Funding

Arthur ORIEUX (salary grant) : MD-PhD student grant – CHU de Bordeaux et Université de Bordeaux

Bourse Société Francophone de Néphrologie Dialyse et Transplantation (SFNDT) 2023

This project is supported by a grant overseen by the French National Research Agency (ANR) as part of the Investment for the Future Programme ANR-18-RHUS-0002 (SHIVA Project) and by the Precision and Global Vascular Brain Health Institute (VBHI) funded by the France 2030 IHU3 initiative

Competing interests

The authors declare no competing interests.

Data Availability

The datasets generated and/or analysed during the current study are available in the ArrayExpress repository number E-MTAB-15937 : https://www.ebi.ac.uk/biostudies/arrayexpress/studies/E-MTAB-15937

References

1. Mills KT, Stefanescu A, He J. The global epidemiology of hypertension. *Nat Rev Nephrol* 2020;**16**:223–237.

2. Zhou B, Perel P, Mensah GA, Ezzati M. Global epidemiology, health burden and effective interventions for elevated blood pressure and hypertension. *Nat Rev Cardiol* 2021;**18**:785–802.

3. Foreman KJ, Marquez N, Dolgert A, Fukutaki K, Fullman N, McGaughey M, Pletcher MA, Smith AE, Tang K, Yuan C-W, Brown JC, Friedman J, He J, Heuton KR, Holmberg M, Patel DJ, Reidy P, Carter A, Cercy K, Chapin A, Douwes-Schultz D, Frank T, Goettsch F, Liu PY, Nandakumar V, Reitsma MB, Reuter V, Sadat N, Sorensen RJD, Srinivasan V, Updike RL, York H, Lopez AD, Lozano R, Lim SS, Mokdad AH, Vollset SE, Murray CJL. Forecasting life expectancy, years of life lost, and all-cause and cause-specific mortality for 250 causes of death: reference and alternative scenarios for 2016–40 for 195 countries and territories. *The Lancet* 2018;**392**:2052–2090.

4. Carey RM, Moran AE, Whelton PK. Treatment of Hypertension: A Review. *JAMA* 2022;**328**:1849.

5. Alexander MR, Edwards TL, Harrison DG. GWAS for Defining the Etiology of Hypertension: Have They Delivered? *Hypertension* 2025:HYPERTENSIONAHA.124.23451.

6. The International Consortium for Blood Pressure Genome-Wide Association Studies. Genetic variants in novel pathways influence blood pressure and cardiovascular disease risk. *Nature* 2011;**478**:103–109.

7. Lerman LO, Kurtz TW, Touyz RM, Ellison DH, Chade AR, Crowley SD, Mattson DL, Mullins JJ, Osborn J, Eirin A, Reckelhoff JF, Iadecola C, Coffman TM, on behalf of the American Heart Association Council on Hypertension and Council on Clinical Cardiology. Animal Models of Hypertension: A Scientific Statement From the American Heart Association. *Hypertension* 2019;**73**.

8. Vorhees CV, Williams MT. Morris water maze: procedures for assessing spatial and related forms of learning and memory. *Nat Protoc* 2006;**1**:848–858.

9. Fox MW. The visual cliff test for the study of visual depth perception in the mouse. *Animal Behaviour* 1965;**13**:232-IN3.

10. Devraj K, Guérit S, Macas J, Reiss Y. An In Vivo Blood-brain Barrier Permeability Assay in Mice Using Fluorescently Labeled Tracers. *JoVE* 2018:57038.

11. Susaki EA, Tainaka K, Perrin D, Yukinaga H, Kuno A, Ueda HR. Advanced CUBIC protocols for whole-brain and whole-body clearing and imaging. *Nat Protoc* 2015;**10**:1709–1727.

12. Schneider CA, Rasband WS, Eliceiri KW. NIH Image to ImageJ: 25 years of image analysis. *Nat Methods* 2012;**9**:671–675.

13. Abelanet A, Camoin M, Rubin S, Bougaran P, Delobel V, Pernot M, Forfar I, Guilbeau-Frugier C, Galès C, Bats ML, Renault M-A, Dufourcq P, Couffinhal T, Duplàa C. Increased Capillary Permeability in Heart Induces Diastolic Dysfunction Independently of Inflammation, Fibrosis, or Cardiomyocyte Dysfunction. *ATVB* 2022;**42**:745–763.

14. Schiller NB, Shah PM, Crawford M, DeMaria A, Devereux R, Feigenbaum H, Gutgesell H, Reichek N, Sahn D, Schnittger I, Silverman NH, Tajik AJ. Recommendations for Quantitation of the Left Ventricle by Two-Dimensional Echocardiography. *Journal of the American Society of Echocardiography* 1989;**2**:358–367.

15. Stypmann J, Engelen MA, Troatz C, Rothenburger M, Eckardt L, Tiemann K. Echocardiographic assessment of global left ventricular function in mice. *Lab Anim* 2009;**43**:127–137.

16. Bats M, Bougaran P, Peghaire C, Gueniot F, Abelanet A, Chan H, Séguy C, Jeanningros S, Jaspard-Vinassa B, Couffinhal T, Duplàa C, Dufourcq P. Therapies targeting Frizzled-7/β-catenin pathway prevent the development of pathological angiogenesis in an ischemic retinopathy model. *The FASEB Journal* 2020;**34**:1288–1303.

17. Emde B, Heinen A, GÃ¶decke A, Bottermann K. Wheat germ agglutinin staining as a suitable method for detection and quantification of fibrosis in cardiac tissue after myocardial infarction. *Eur J Histochem* 2014.

18. Gueniot F, Rubin S, Bougaran P, Abelanet A, Morel JL, Bontempi B, Proust C, Dufourcq P, Couffinhal T, Duplàa C. Targeting *Pdzrn3* maintains adult blood-brain barrier and central nervous system homeostasis. *J Cereb Blood Flow Metab* 2022;**42**:613–629.

19. Lee Y-K, Uchida H, Smith H, Ito A, Sanchez T. The isolation and molecular characterization of cerebral microvessels. *Nat Protoc* 2019;**14**:3059–3081.

20. Robinson MD, McCarthy DJ, Smyth GK. edgeR : a Bioconductor package for differential expression analysis of digital gene expression data. *Bioinformatics* 2010;**26**:139–140.

21. Wolf G, Lotan A, Lifschytz T, Ben-Ari H, Kreisel Merzel T, Tatarskyy P, Valitzky M, Mernick B, Avidan E, Koroukhov N, Lerer B. Differentially Severe Cognitive Effects of Compromised Cerebral

Blood Flow in Aged Mice: Association with Myelin Degradation and Microglia Activation. *Front Aging Neurosci* 2017;**9**:191.

22. Di Pardo A, Amico E, Scalabrì F, Pepe G, Castaldo S, Elifani F, Capocci L, De Sanctis C, Comerci L, Pompeo F, D'Esposito M, Filosa S, Crispi S, Maglione V. Impairment of blood-brain barrier is an early event in R6/2 mouse model of Huntington Disease. *Sci Rep* 2017;**7**:41316.

23. Kelly DM, Rothwell PM. Blood pressure and the brain: the neurology of hypertension. *Pract Neurol* 2020;**20**:100–108.

24. Escartin C, Galea E, Lakatos A, O'Callaghan JP, Petzold GC, Serrano-Pozo A, Steinhäuser C, Volterra A, Carmignoto G, Agarwal A, Allen NJ, Araque A, Barbeito L, Barzilai A, Bergles DE, Bonvento G, Butt AM, Chen W-T, Cohen-Salmon M, Cunningham C, Deneen B, De Strooper B, Díaz-Castro B, Farina C, Freeman M, Gallo V, Goldman JE, Goldman SA, Götz M, Gutiérrez A, Haydon PG, Heiland DH, Hol EM, Holt MG, Iino M, Kastanenka KV, Kettenmann H, Khakh BS, Koizumi S, Lee CJ, Liddelow SA, MacVicar BA, Magistretti P, Messing A, Mishra A, Molofsky AV, Murai KK, Norris CM, Okada S, Oliet SHR, Oliveira JF, Panatier A, Parpura V, Pekna M, Pekny M, Pellerin L, Perea G, Pérez-Nievas BG, Pfrieger FW, Poskanzer KE, Quintana FJ, Ransohoff RM, Riquelme-Perez M, Robel S, Rose CR, Rothstein JD, Rouach N, Rowitch DH, Semyanov A, Sirko S, Sontheimer H, Swanson RA, Vitorica J, Wanner I-B, Wood LB, Wu J, Zheng B, Zimmer ER, Zorec R, Sofroniew MV, Verkhratsky A. Reactive astrocyte nomenclature, definitions, and future directions. *Nat Neurosci* 2021;**24**:312–325.

25. Wang G, Lai FM-M, Kwan BC-H, Lai K-B, Chow K-M, Li PK-T, Szeto C-C. Podocyte Loss in Human Hypertensive Nephrosclerosis. *American Journal of Hypertension* 2009;**22**:300–306.

26. Xue B, Pamidimukkala J, Hay M. Sex differences in the development of angiotensin II-induced hypertension in conscious mice. *American Journal of Physiology-Heart and Circulatory Physiology* 2005;**288**:H2177–H2184.

27. Benigni A, Cassis P, Remuzzi G. Angiotensin II revisited: new roles in inflammation, immunology and aging. *EMBO Mol Med* 2010;**2**:247–257.

28. Guzik TJ, Nosalski R, Maffia P, Drummond GR. Immune and inflammatory mechanisms in hypertension. *Nat Rev Cardiol* 2024;**21**:396–416.

29. González Ibanez F, Picard K, Bordeleau M, Sharma K, Bisht K, Tremblay M-È. Immunofluorescence Staining Using IBA1 and TMEM119 for Microglial Density, Morphology and Peripheral Myeloid Cell Infiltration Analysis in Mouse Brain. *JoVE* 2019:60510.

30. Wen W, Cheng J, Tang Y. Brain perivascular macrophages: current understanding and future prospects. *Brain* 2024;**147**:39–55.

31. Faraco G, Sugiyama Y, Lane D, Garcia-Bonilla L, Chang H, Santisteban MM, Racchumi G, Murphy M, Van Rooijen N, Anrather J, Iadecola C. Perivascular macrophages mediate the neurovascular and cognitive dysfunction associated with hypertension. *Journal of Clinical Investigation* 2016;**126**:4674–4689.

32. Pantoni L. Cerebral small vessel disease: from pathogenesis and clinical characteristics to therapeutic challenges. *The Lancet Neurology* 2010;**9**:689–701.

33. Hainsworth AH, Markus HS, Schneider JA. Cerebral Small Vessel Disease, Hypertension, and Vascular Contributions to Cognitive Impairment and Dementia. *Hypertension* 2024;**81**:75–86.

34. Gallo G, Volpe M, Savoia C. Endothelial Dysfunction in Hypertension: Current Concepts and Clinical Implications. *Front Med* 2022;**8**:798958.

35. Quick S, Moss J, Rajani RM, Williams A. A Vessel for Change: Endothelial Dysfunction in Cerebral Small Vessel Disease. *Trends in Neurosciences* 2021;**44**:289–305.

36. Mora P, Hollier P-L, Guimbal S, Abelanet A, Diop A, Cornuault L, Couffinhal T, Horng S, Gadeau A-P, Renault M-A, Chapouly C. Blood–brain barrier genetic disruption leads to protective barrier formation at the Glia Limitans. Daneman R, ed. *PLoS Biol* 2020;**18**:e3000946.

37. Haruwaka K, Ikegami A, Tachibana Y, Ohno N, Konishi H, Hashimoto A, Matsumoto M, Kato D, Ono R, Kiyama H, Moorhouse AJ, Nabekura J, Wake H. Dual microglia effects on blood brain barrier permeability induced by systemic inflammation. *Nat Commun* 2019;**10**:5816.

38. Harrison DG, Patrick DM. Immune Mechanisms in Hypertension. *Hypertension* 2024;**81**:1659–1674.

Author Contribution Statement

Data acquisition : Maxime Michot, Juliette Vaurs, Marie-Lise Bats, Virginie Dinet, Romain Boulestreau
Data acquisition, analysis and interpretation of data : Arthur Orieux Marie-Lise Bats and Sébastien Rubin
Conception or design of the work : Sébastien Rubin, Cécile Duplaa, Thierry Couffinhal
Drafting the work : Arthur Orieux and Sébastien Rubin
Reviewing the manuscript Sébastien Rubin, Cécile Duplaa, Thierry Couffinhal, Alexandre Boyer, Claire Peghaire and Pascale Dufourcq
Important intellectual content : Sébastien Rubin, Cécile Duplaa, Thierry Couffinhal, Claire Peghaire